# DETECTION OF SANDBANKS USING SYNTHETIC APERTURE RADAR IMAGES TIME SERIES

*José Alberto Silva de Sá[1], Fábio Furlan Gama[2], José Claudio Mura[2], Gilberto Ribeiro de Queiroz[2], Lúbia Vinhas[2] and Brígida Ramati Pereira da Rocha[3]*

[1]Universidade do Estado do Pará (UEPA), Tv. Doutor Enéas Pinheiro, 2626, Belém–PA–Brasil, josealbertosa@uepa.br;
[2]Instituto Nacional de Pesquisas Espaciais (INPE), Av. dos Astronautas, 1758, São José dos Campos–SP–Brasil, fabio.furlan@inpe.br, jose.mura@inpe.br, gilberto.queiroz@inpe.br, lubia.vinhas@inpe.br;
[3]Universidade Federal do Pará (UFPA), Rua Augusto Corrêa, 1, Belém–PA–Brasil, brigida@ufpa.br

## ABSTRACT

A sandbank consists of the accumulation of sediments (sand and gravel) deposited in a riverbed or along the coast, constituting an obstacle to navigation. This work aimed to develop a technique for the detection of sandbanks located in an Amazonian estuarine region (Guajará's bay) using synthetic aperture radar images time series in order to assist the obstacles monitoring in the local navigation. We used 28 images of the Sentinel-1 Mission; Orbital Platform: S1A; Band: C; Product Type: Ground Range Detected (GRDH); Polarizations: VV and VH; Sensor Mode: Interferometric Wide Swath Mode (IW). The results showed a significant stratification for 3 classes (Water, Sandbank and River Island), with accuracy equal to 91,1% for an automatic classification by the k-NN algorithm.

***Key words*** — Synthetic aperture radar, time series, sandbank, Amazon region.

## 1. INTRODUCTION

Sandbanks are a danger to navigation (river and sea), and can cause damage and shipwrecks. In the Amazon region, the river network is one of the main ways of access to municipalities and communities, and sandbanks are a significant problem for those who travel in Amazonian rivers. In order to help the quality of navigation in this region, the objective of this work was to develop a technique to aid the detection of sandbanks and changes in the delimitations of the coastlines, in order to collaborate with the updating of nautical charts which have an important role for river and maritime navigation.

The survey of sandbank areas is generally difficult (risk to vessels) and costly (logistic costs associated with bathymetry), resulting in a limited amount of data that can be obtained by traditional techniques. Alternatively, remote sensing techniques provide effective and safe tools for making inferences and ancillary indications to large spatial measurement processes. Synthetic Aperture Radar (SAR), in particular, is a promising medium for monitoring the temporal evolution of sandbanks, mainly due to their advantages in operational capacity, to generate significant products regardless of weather, besides allowing surveillance for a wide area [1], [2].

The European Space Agency's Copernicus Program aims to produce long-term SAR data through the Sentinel Missions to support different applications based on time series [3], [4], [5]. Open access to Sentinel-1 mission data, consisting of two polar orbiting satellites that generate SAR images in the C band, is now a significant source of data for the monitoring of targets in the Amazon region. The Sentinel-1 Mission is designed to provide high space-time resolution for operational services and applications that require long time series of terrestrial data, with each satellite in the Sentinel-1 constellation transmitting Earth observation data for at least 7 years (with energy resources for 12 years), and for the Amazon region the time to revisit is 12 days.

The objective of this exploratory-descriptive study was to propose a technique for the automatic detection of sandbanks in rivers using synthetic aperture radar images time series.

## 2. MATERIAL AND METHODS

### 2.1. Area of study: Guajará's Bay

The technique was tested in Guajara's bay, in the confluence of the rivers Guamá and Acará, in Pará State, Brazil.

### 2.2. SAR data

We used all SAR images of the Sentinel-1 mission (28 scenes), available at the ESA Copernicus Open Access Hub, for the study area in the year 2017, with specifications: Orbital Platform: S1A; Band: C; Product Type: Ground Range Detected (GRDH); Polarizations: VV and VH; Sensor Mode: Interferometric Wide Swath Mode (IW).

Table 1 shows the names of the all products used in this study.

### 2.3. Processing of the SAR images

The software Sentinel Application Platform (SNAP) was used in the processing of the SAR images, being extracted from each scene a subset containing 3 targets (water, sandbank and river island). Subsequently, each subset

received radiometric calibration, speckle filtering, geocoding and stacking.

| |
|---|
| S1A_IW_GRDH_1SDV_20170110T085732_20170110T085757_014767_0180B6_919D |
| S1A_IW_GRDH_1SDV_20170122T085731_20170122T085756_014942_018638_7C02 |
| S1A_IW_GRDH_1SDV_20170203T085731_20170203T085756_015117_018B7D_8FAF |
| S1A_IW_GRDH_1SDV_20170215T085731_20170215T085756_015292_019107_5C3B |
| S1A_IW_GRDH_1SDV_20170227T085731_20170227T085756_015467_01965D_177D |
| S1A_IW_GRDH_1SDV_20170311T085732_20170311T085757_015642_019BAA_B086 |
| S1A_IW_GRDH_1SDV_20170323T085732_20170323T085757_015817_01A0DD_2C8F |
| S1A_IW_GRDH_1SDV_20170404T085732_20170404T085757_015992_01A60D_0CA4 |
| S1A_IW_GRDH_1SDV_20170416T085733_20170416T085758_016167_01AB6A_C5CE |
| S1A_IW_GRDH_1SDV_20170428T085733_20170428T085758_016342_01B0B9_4AB8 |
| S1A_IW_GRDH_1SDV_20170510T085734_20170510T085759_016517_01B605_AF6B |
| S1A_IW_GRDH_1SDV_20170522T085734_20170522T085759_016692_01BB69_C3D6 |
| S1A_IW_GRDH_1SDV_20170603T085735_20170603T085800_016867_01C0D2_A120 |
| S1A_IW_GRDH_1SDV_20170615T085736_20170615T085801_017042_01C638_6975 |
| S1A_IW_GRDH_1SDV_20170627T085737_20170627T085802_017217_01CB8D_2DEC |
| S1A_IW_GRDH_1SDV_20170709T085737_20170709T085802_017392_01D0D1_344D |
| S1A_IW_GRDH_1SDV_20170721T085738_20170721T085803_017567_01D624_0D11 |
| S1A_IW_GRDH_1SDV_20170802T085739_20170802T085804_017742_01DB7F_B1D9 |
| S1A_IW_GRDH_1SDV_20170814T085739_20170814T085804_017917_01E0D1_07AD |
| S1A_IW_GRDH_1SDV_20170826T085740_20170826T085805_018092_01E61D_9A0D |
| S1A_IW_GRDH_1SDV_20170907T085740_20170907T085805_018267_01EB6E_CC5F |
| S1A_IW_GRDH_1SDV_20170919T085741_20170919T085806_018442_01F0D6_4F70 |
| S1A_IW_GRDH_1SDV_20171001T085741_20171001T085806_018617_01F63B_3CE7 |
| S1A_IW_GRDH_1SDV_20171013T085741_20171013T085806_018792_01FB8D_03E3 |
| S1A_IW_GRDH_1SDV_20171118T085741_20171118T085806_019317_020BBD_8EB0 |
| S1A_IW_GRDH_1SDV_20171130T085741_20171130T085806_019492_021136_15BC |
| S1A_IW_GRDH_1SDV_20171212T085740_20171212T085805_019667_0216B4_BB84 |
| S1A_IW_GRDH_1SDV_20171224T085740_20171224T085805_019842_021C14_699E |

**Table 1. Names of the Sentinel-1 products used in this study.**

Figure 1 shows a processed subset of the product S1A_IW_GRDH_1SDV_20170311T085732_20170311T085757_015642_019BAA_B086, with acquisition date on 11/03/2017, at a time when the tide height was 0.2 m above the reduction level (Port of Belém). Significant difference in sigma nought (brightness) is observed for the sandbank target in the VH and VV polarizations (red arrows). This fact is explained by the Bragg effect [6].

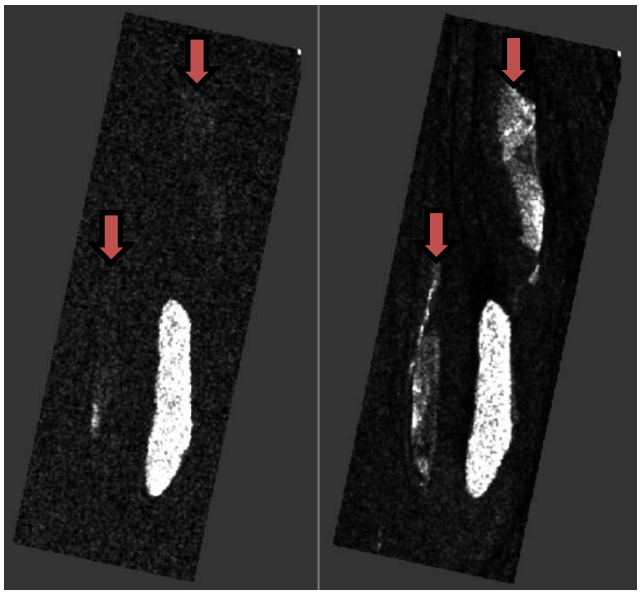

**(a)** **(b)**

**Figure 1. (a) Sigma-nought VH and (b) Sigma-nought VV.**

## 2.4. Time series sampling

Scattering coefficient time series samples (per pixel), in the VH and VV polarizations, were collected randomly for each target (water, sandbank and river island), being 60 samples of each, thus totaling 180 samples. Then, the mean values and standard deviations of each sample were obtained. Figure 2 shows a time series visualization of each target, for the VH and VV polarizations. In general, we noticed differences in the basic configuration of the time series.

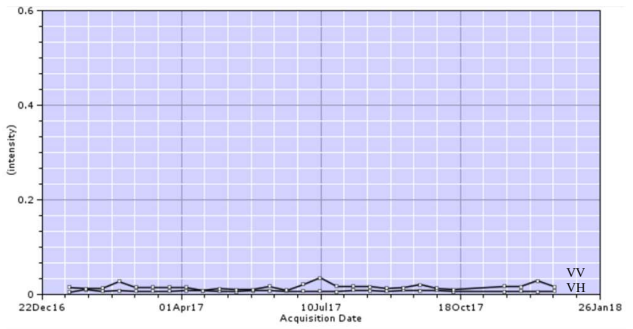


**(a)**

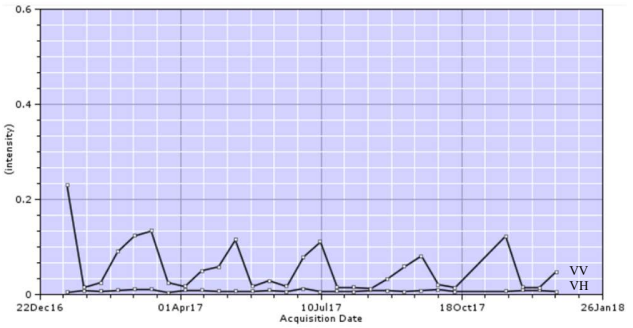


**(b)**

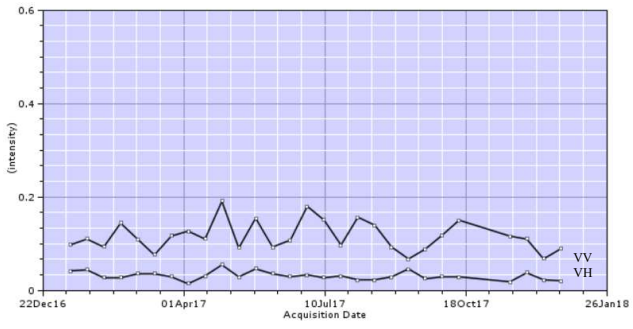


**(c)**

**Figure 2. Time series visualization of each target, for the VH and VV polarizations: (a) water, (b) sandbank and (c) river island.**

### 2.5. Targets classification by k-NN algorithm

We randomly selected 135 time series to compose the training data set (75% of the total data), with 45 examples of each target (water, sandbank and river island). The remaining data, therefore 45 time series, were used for the composition of the test data set (25% of the total data), with 15 examples of each target. In this way, we used balanced data. The predictive variables were the following indexs:

$$Q_1 = \frac{\mu_{VH}}{\mu_{VV}} \qquad Q_2 = \frac{\sigma_{VH}}{\sigma_{VV}}$$

Where:
$\mu_{VH}$ is the scattering coefficient average in the VH polarization.
$\mu_{VV}$ is the scattering coefficient average in the VV polarization.
$\sigma_{VH}$ is the scattering coefficient standard deviation in the VH polarization.
$\sigma_{VV}$ is the scattering coefficient standard deviation in the VV polarization.

The k-NN (k-Nearest Neighbors) classifier was designed for k = 5 using the Euclidean distance as the metric.

## 3. RESULTS

The k-NN classifier obtained predictive accuracy equal to 91.1%. Figure 3 shows the confusion matrix for the three targets studied.

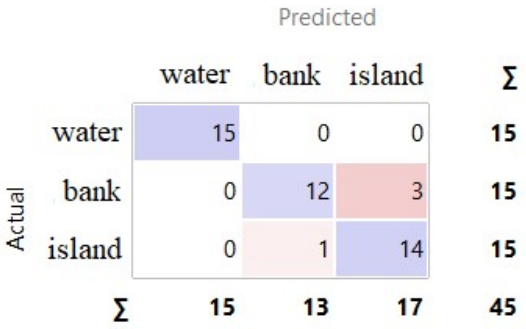


**Figure 3. Confusion matrix for the three targets studied.**

Figure 4 shows the scatter plot with class density for the $Q_1$ and $Q_2$ indexs. There are stratification zones for the targets (water, sandbank and river island).

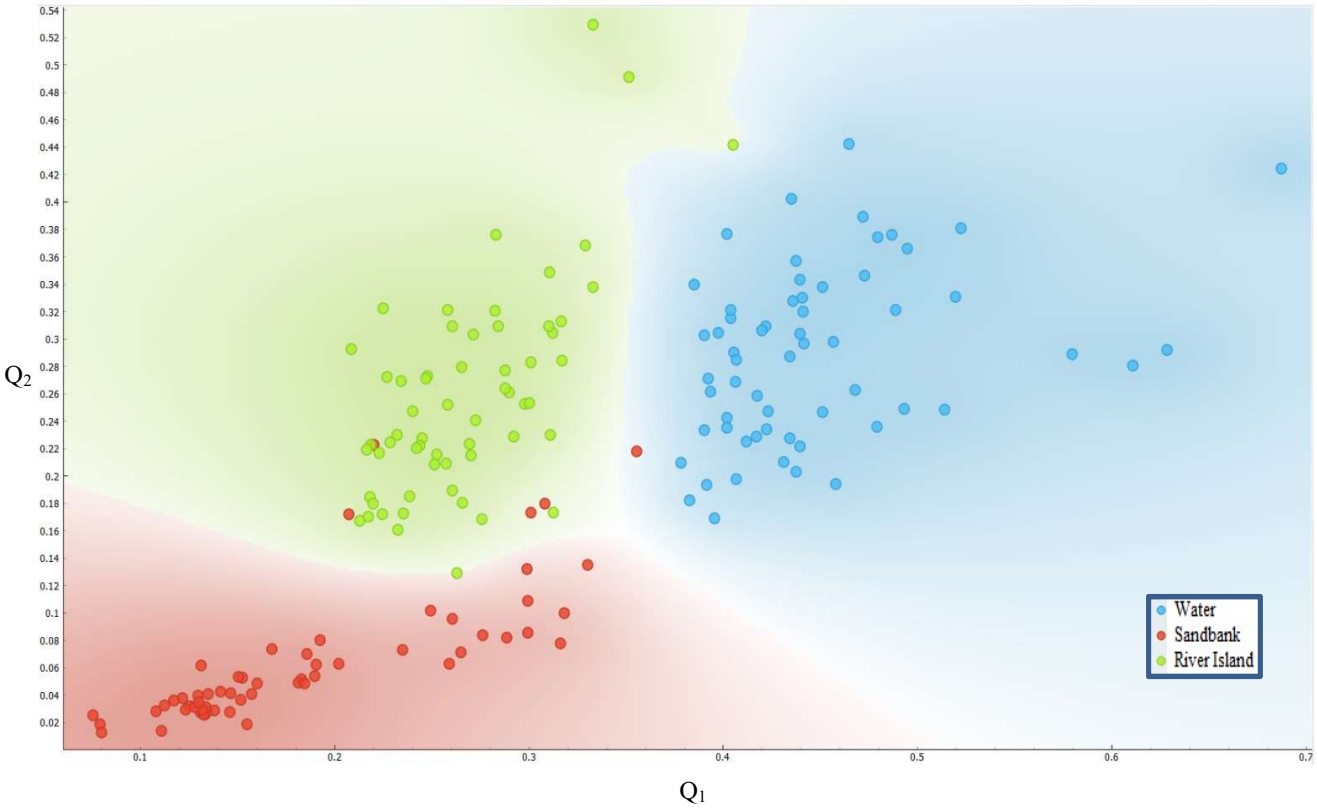


**Figure 4. Scatter plot with class density for the $Q_1$ and $Q_2$ indexs.**

## 4. CONCLUSIONS

This study had the following conclusions:

a) SAR images of the Mission Sentinel-1 obtained with the VV polarization showed better detection of sandbank when comparing the SAR images obtained with the VH polarization, this being explained by the Bragg effect;

b) Analysis of the $Q_1$ and $Q_2$ indexs allowed the identification of stratification zones for the targets (water, sandbank and river island);

c) The propused $Q_1$ and $Q_2$ indexs were also used as input attributes for the k-NN classifier algorithm, obtaining an accuracy equal to 91.1% for automatic target detection. The proposed technique is in phase of consolidation, requiring further studies in other Amazonian estuarine regions.

## 5. ACKNOWLEDGMENT

The authors would like to thank European Space Agency's Copernicus Program for the open access of SAR images of the Sentinel-1 mission.

## 6. REFERENCES

[1] Cheng, T. et al. “Sandbank and Oyster Farm Monitoring with Multi-Temporal Polarimetric SAR Data Using Four-Component Scattering Power Decomposition”, IEICE TRANS. COMMUN. pp. 2573-2579, 2013.

[2]_Yang, J. et al. “Review of the study on the underwater topography detection with sar imagery in sino-european dragon cooperation programme”, ESA-SP Vol. 655, ISBN: 98-92-9221-219-3., pp.10, 2008.

[3] EUROPEAN SPACE AGENCY. “Copernicus: Overview”, http://www.esa.int/Our_Activities/Observing_the_Earth/Copernicus/Overview3, 2018.

[4] EUROPEAN SPACE AGENCY. “Sentinel Missions”, https://sentinel.esa.int/web/sentinel/missions, 2018.

[5] EUROPEAN SPACE AGENCY. “Acquisition Modes”, https://sentinel.esa.int/web/sentinel/technical-guides/sentinel-1-sar, 2018.

[6] Violante-Carvalho, N. “Sobre os mecanismos de imageamento do radar de abertura sintética SAR para a estimação do espectro direcional de ondas geradas pelo vento”, Revista Brasileira de Geofísica. pp. 593-607, 2010.